self-diffusivities of 1.1×10^{-8} and 1.25×10^{-9} m^2 s^{-1} were obtained. Hence it turns out that in the mixture the difference in the mobility of the two components is much less than for single-component adsorption. Such behavior is well-known from the investigation of multicomponent liquids[7,8] and may be understood as a consequence of the interaction between the different diffusants. It is interesting to note that in comparison to single-component adsorption the diffusivity of ethene remains essentially unchanged, while the ethane diffusivity is distinctly reduced. One has to conclude, therefore, that encounters between unlike molecules within the intracrystalline pore system predominantly reduce the mobility of the (more mobile) ethane molecules rather than enhance the mobility of the (more strongly bounded) ethene molecules.

Under the assumption that no additional transport resistance ("surface barriers"[2,19]) exists at the external surface of the zeolite crystallites, the mean intracrystalline residence time may be easily calculated from the size of the crystallites and the coefficient of intracrystalline self-diffusion.[4] For crystallites of spherical shape (which generally is a sufficiently good approximation) one has[2,4,13]

$$\tau_{\text{intra}}^{\text{D}} = \langle R^2 \rangle / 15 D_{\text{intra}} \qquad (7)$$

where $\langle R^2 \rangle$ denotes the mean square crystallite radius. Inserting the intracrystalline diffusivities determined by PFG Fourier transform NMR for the two components into eq 7 yields values of 13.5 and 48 ms, respectively. These data are in satisfactory agreement with the values for the real intracrystalline mean lifetimes τ_{intra} following from the NMR tracer desorption curves represented in Figure 3. One has to conclude, therefore, that for either of the adsorbed components the crystallite surface does not exert any significant transport resistance. This result is in agreement with previous single-component PFG NMR investigations[13,15] where, in contrast to the small pore A type zeolites, the more open NaX structure was found to show no tendency to forming surface barriers.

(19) Bülow, M. *Z. Chem.* **1985**, *25*, 81.

Conclusion

PFG Fourier transform NMR has been successfully applied to measure selectively the self-diffusion coefficients in a two-component mixture adsorbed on microporous adsorbents.

In an ethane–ethene mixture adsorbed on zeolite NaX the diffusivity of the ethene molecules is by a factor of 3 to 4 smaller than the mobility of ethane. This result may be understood as a consequence of the specific interaction of the unsaturated hydrocarbons with the sodium cations. As a consequence of the mutual interaction between the two components this difference is distinctly smaller than that for single-component adsorption. The values for the mean intracrystalline residence times of both components estimated from these intracrystalline diffusivities are in satisfactory agreement with the results directly determined by NMR tracer desorption studies. This experimental finding provides an independent check of the correctness of the measured diffusivities, and in agreement with previous studies, a significant influence of additional transport resistances on the outer surface of the crystallites (surface barriers) may be excluded.

Resonance Raman Studies of Oxycytochrome P450cam: Effect of Substrate Structure on ν(O–O) and ν(Fe–O_2)

Songzhou Hu, Andrew J. Schneider, and James R. Kincaid*

Contribution from the Chemistry Department, Marquette University, Milwaukee, Wisconsin 53233. *Received September 17, 1990*

Abstract: Resonance Raman spectra of dioxygen adducts of cytochrome P450cam, in the presence of various substrates, and their biomimetic analogues are reported. The oxidation marker band, ν_4, of oxycytochrome P450cam is observed at 1374 cm^{-1}, which is lower than that of oxyhemeproteins possessing histidyl as a proximal ligand, reflecting the presence of a strong electron-releasing thiolate axial ligand. Both the ν(O–O) and ν(Fe–O_2) modes are simultaneously observed and identified (by using $^{16}O_2/^{18}O_2$ isotopic substitution technique) at 1140 cm^{-1} and 541 cm^{-1}, respectively for camphor-bound oxygenated cytochrome P450cam. When camphor is replaced with adamantanone, two lines at 1139 cm^{-1} and 1147 cm^{-1} are observed for the ν(O–O) mode, while no significant change in heme core structure is discerned. The substantially lowered frequencies of the ν(O–O) and ν(Fe–O_2) and their sensitivity to the variation of the substrate structure provide a structural basis for cleavage of the bound dioxygen to generate a regio- and stereospecific hydroxylation agent.

Introduction

Cytochrome P450 includes a number of b-type heme proteins that have a characteristic electronic absorption band at 450 nm when combined with carbon monoxide in the reduced state.[1] They occur in many types of mammalian tissue, plants, and microorganisms and catalyze the incorporation of one atom of molecular oxygen into a vast variety of hydrophobic substances.[2] Because of their novel catalytic properties in the activation of dioxygen, they have received considerable attention in the past.[3] Among various cytochromes P450 that have been isolated, the water-soluble, three-component cytochrome P450 monoxygenase system, induced by camphor and isolated from the bacterium *Pseudomonas putida*, has been the most extensively characterized,[4] owing to its relative ease of handling. The recent X-ray crystallographic

(1) (a) Ortiz de Montellano, P. R., Ed. *Cytochrome P450 Structure, Mechanism, and Biochemistry*; Plenum Press: New York, 1986. (b) Schuster, I., Ed. *Cytochrome P450: Biochemistry and Biophysics*; Taylor & Francis: London, 1989. (c) Sato, R.; Omura, T., Eds.; *Cytochrome P450*; Academic Press: New York, 1978.

(2) (a) Black, S. D.; Coon, M. J. *Adv. Enzymol. Relat. Areas Mol. Biol.* **1987**, *60*, 35-87. (b) White, R. E.; Coon, M. J. *Annu. Rev. Biochem.* **1980**, *49*, 315.

(3) (a) Dawson, J. H.; Eble, K. S. *Adv. Inorg. Bioinorg. Mech.* **1986**, *4*, 1-64. (b) Murray, R. I.; Fisher, M. T.; Debrunner, G.; Sligar, S. G. In *Metalloproteins. Part I: Metal Proteins with Redox Roles*; Harrison, P. M., Ed.; Verlag Chemie: Weinheim, 1985; p 157. (c) Dawson, J. H. *Science* **1988**, *240*, 433-439. (d) Guengerich, F. P.; McDonald, T. L. *Acc. Chem. Res.* **1984**, *17*, 9-16. (e) Dawson, J. H.; Sono, M. *Chem. Rev.* **1987**, *87*, 1255-1276. (f) Lewis, D. F. V. *Drug Metab. Rev.* **1986**, *17*, 1-66.

(4) (a) Sligar, S. G.; Gelb, M. H.; Heimbrook, D. C. *Xenobiotica* **1984**, *14*, 63-86. (b) Poulos, T. L. *Pharm. Rev.* **1988**, *5*, 67-75. (c) Champion, P. M. In *Biological Application of Raman Spectroscopy*; Spiro, T. G., Ed.; John Wiley: New York, 1989; Vol. 3, pp 249-292.

0002-7863/91/1513-4815$02.50/0

studies[5] of this camphor hydroxylase, known as P450cam, have defined the molecular structure and provided a solid foundation toward the understanding of its catalytic mechanism. They reveal unambiguously the presence of a unique Fe–S linkage in the substrate-free, camphor-bound, and CO-liganded forms, which had been suggested from numerous spectroscopic studies and biomimetic modeling.

Mechanistic studies on this system have established that cytochrome P450cam initiates the biological degradation of camphor through the stereo- and regiospecific hydroxylation of its substrate at the 5-exo position, with four spectrally discernible species being involved. The low-spin ferric resting enzyme is converted to the high-spin state upon the binding of camphor. Reduction of this species results in the formation of a five-coordinated, high-spin ferrous cytochrome P450cam, which then binds molecular oxygen reversibly to form a quasi-stable oxygenated cytochrome P450cam. The transfer of an electron from reduced putidaredoxin (the essential iron–sulfur protein redox partner) to oxycytochrome P450cam leads to the cleavage of the bound dioxygen and concomitant hydroxylation of camphor without observation of an intermediate.[6] Of these reactive intermediates, the last one, i.e., oxygenated cytochrome P450cam, is of particular interest, since it shows a completely different reactivity when compared with the dioxygen adducts of other hemeproteins. For example, the oxygen transport hemeproteins such as hemoglobin and myoglobin bind oxygen passively, leaving the O–O bond intact, while cytochrome *c* oxidase reduces the bound oxygen to water.[7] Though several physical techniques[8] have been applied to study this key intermediate, specific structural characteristics remain ill-defined.

Resonance Raman (RR) spectroscopy is a very powerful technique for elucidating the active site structure of hemeproteins[9] and has played a vital role in the understanding of cytochrome P450 from various sources.[10] In the RR spectrum of the reduced ferrous state, the π-electron density marker band (ν_4) is invariably located at 1341 to 1346 cm^{-1}, which is approximately 10 cm^{-1} lower than those observed for high-spin ferrous hemeproteins possessing a histidyl proximal ligand. This behavior is consistent with the presence of a strong electron-donating axial ligand such as mercaptide. The enhancement of the Fe–S stretching mode at 351 cm^{-1}, identified through isotopically enriched (^{54}Fe, ^{34}S) and natural abundance (^{56}Fe, ^{32}S) cytochrome P450cam,[11] provided decisive evidence for a Fe–S linkage in the high-spin ferric state. Furthermore, the RR detection of axial vibrational modes of the ferrous carbon monoxide adducts[12] and the ferric nitric oxide adducts[13] has shed light on the interaction of substrates with the bound ligand at the active site. Even more interesting is the unprecedented RR enhancement of the internal O–O stretching mode for oxygenated cytochrome P450cam[14] and its model compound.[15] However, the key ν(Fe–O_2) mode, which carries much information about the bond strength and geometry of the Fe–O_2 linkage, has thus far eluded detection.

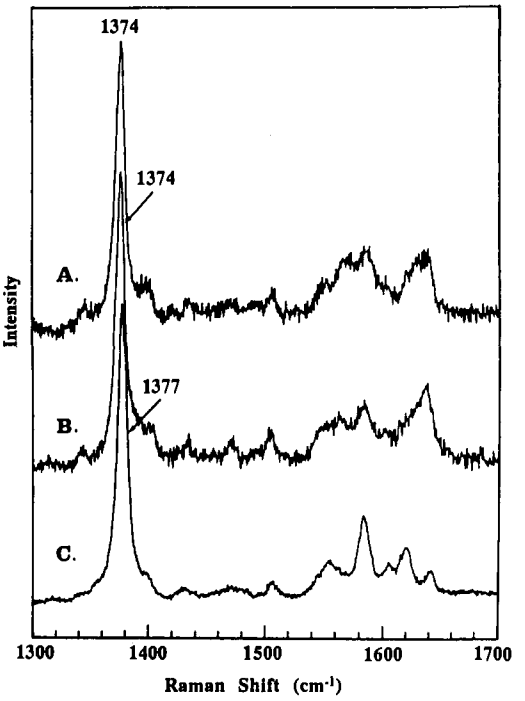

Figure 1. High-frequency resonance Raman spectra of the frozen solution of oxygenated cytochrome P450cam in the presence of 1 mM camphor (trace A) and saturated adamantanone (trace B) as well as oxymyoglobin (trace C) at −80 °C.

In this paper, we report resonance Raman spectroscopic characterization of oxygenated cytochrome P450cam in the presence of various substrates. The ν(O–O) and ν(Fe–O_2) modes are simultaneously observed at 1140 cm^{-1} and 541 cm^{-1} for the dioxygen adduct of camphor-bound P450cam. In addition, we provide the first direct evidence for the interaction of the bound dioxygen with substrate, camphor, a feature that has been proposed from the model construction based on the high-resolution X-ray crystal structure of cytochrome P450cam[5c] and RR studies of the carbon monoxide[12] and nitric oxide[13] adducts in various substrate-bound states. The significantly lowered frequencies of ν(Fe–O_2) and ν(O–O) and their sensitivity to substrate replacement provide a structural basis for cleavage of the bound dioxygen to generate a regio- and stereospecific hydroxylation agent.

Experimental Section

Cytochrome P450cam was isolated and purified by the method of Gunsalus and Wagner[16] with slight modification. Instead of ammonium sulfate fractionation, the crude enzyme, eluted from the first DE-52 (Whatman) ion-exchange column, was concentrated and passed over an 80 × 5 cm Biogel (Bio-Rad) column repetitively to bring the Rz value (391-nm absorbance/280-nm absorbance) to 1.1. The Biogel P100 column was previously equilibrated with 20 mM potassium phosphate

(5) (a) Poulos, T. L.; Finzel, B. C.; Gunsalus, I. C.; Wagner, G. C.; Kraut, J. *J. Biol. Chem.* **1985**, *260*, 16122–16130. (b) Poulos, T. L.; Finzel, B. C.; Howard, A. J. *Biochemistry* **1986**, *25*, 5314. (c) Poulos, T. L.; Finzel, B. C.; Howard, A. J. *J. Mol. Biol.* **1987**, *195*, 687–700. (d) Raag, R.; Poulos, T. L. *Biochemistry* **1989**, *28*, 917–922. (e) Raag, R.; Poulos, T. L. *Biochemistry* **1989**, *28*, 7586–7592.

(6) (a) Brewer, C. B.; Peterson, J. A. *J. Biol. Chem.* **1988**, *263*, 791–798. (b) Brewer, C. B.; Peterson, J. A. *Arch. Biochem. Biophys.* **1986**, *249*, 515–521. (c) Lipscomb, J. D.; Sligar, S. G.; Namtvedt, M. J.; Gunsalus, I. C. *J. Biol. Chem.* **1976**, *251*, 1116–1124. (d) Hui Bon Hoa, G.; Begard, E.; Debey, P.; Gunsalus, I. C. *Biochemistry* **1978**, *17*, 2835.

(7) (a) Naqui, A.; Chance, B. *Annu. Rev. Biochem.* **1986**, *55*, 137. (b) Capaldi, R. A. *Annu. Rev. Biochem.* **1990**, *59*, 569–596.

(8) Dawson, J. H.; Kau, L. S.; Penner-Hahn, J. E.; Sono, M.; Eble, K. S.; Bruce, G. S.; Hager, L. P.; Hodgson, K. O. *J. Am. Chem. Soc.* **1986**, *108*, 8114.

(9) Spiro, T. G., Ed. *Biological Applications of Raman Spectroscopy*; John Wiley: New York, 1988; Vol. 3.

(10) (a) Ozaki, Y.; Kitagawa, T.; Kyogoku, Y.; Shimada, H.; Iizuka, T.; Ishimura, Y. *J. Biochem.* **1976**, *80*, 1447–1457. (b) Champion, P. M.; Gunsalus, I. C.; Wagner, G. C. *J. Am. Chem. Soc.* **1978**, *100*, 3743–3751. (c) Bangchaoenpaurpong, O.; Champion, P. M.; Martinis, S. A.; Sligar, S. A. *J. Chem. Phys.* **1987**, *87*, 4273–4284. (d) Anzenbacher, P.; Evangelista-Kirp, R.; Schenkman, J.; Spiro, T. G. *Inorg. Chem.* **1989**, *28*, 4491–4495. (e) Shimizu, T.; Kitagawa, T.; Mitani, F.; Iizuka, T.; Ishimura, Y. *Biochim. Biophys. Acta* **1981**, *670*, 236–242. (f) Ozaki, Y.; Kitagawa, T.; Kyogoku, Y.; Imai, Y.; Hashimoto-Yutsudo, C.; Sato, R. *Biochemistry* **1978**, *17*, 5826–5831. (g) Tsubaki, M.; Hiwatashi, A.; Ichikawa, Y. *Biochemistry* **1987**, *26*, 4535–4540. (h) Hildebrandt, P.; Garda, H.; Stier, A.; Stockburger, M.; Van Dyke, R. A. *FEBS Lett.* **1988**, *237*, 15–20. (i) Kelly, K.; Rospendowski, B. N.; Smith, W. E.; Wolf, C. R. *FEBS Lett.* **1987**, *222*, 120–124. (j) Hildebrandt, P.; Greinert, R.; Stier, A.; Taniguchi, H. *Eur. J. Biochem.* **1989**, *186*, 291–302. (k) Hildebrandt, P.; Garda, H.; Stier, A.; Bachmanova, G. I.; Kanaeva, I. P.; Archakov, A. I. *Eur. J. Biochem.* **1989**, *186*, 383–388.

(11) Champion, P. M.; Stallard, B. R.; Wagner, G. C.; Gunsalus, I. C. *J. Am. Chem. Soc.* **1982**, *104*, 5469–5472.

(12) (a) Uno, T.; Nishimura, Y.; Makino, R.; Iizuka, T.; Ishimura, Y.; Tsubol, M. *J. Biol. Chem.* **1985**, *260*, 2023–2026. (b) Tsubol, M. *Indian J. Pure Appl. Phys.* **1988**, *26*, 188–191.

(13) Hu, S.; Kincaid, J. R. *J. Am. Chem. Soc.* **1991**, *113*, 2843–2850.

(14) Bangchaoenpaurpong, O.; Rizos, A. K.; Champion, P. M.; Jollie, D.; Sligar, S. *J. Biol. Chem.* **1986**, *261*, 8089–8092.

(15) Chottard, G.; Schappacher, M.; Ricard, L.; Weiss, R. *Inorg. Chem.* **1984**, *23*, 4557–4561.

(16) Gunsalus, I. C.; Wagner, G. C. *Methods Enzymol.* **1978**, *52*, 166–188.

buffer (pH = 7.4) containing 100 mM KCl and 1 mM camphor. The partially purified protein was further chromatographed on a 2.5 × 20 DEAE-Sephadex (Pharmacia) column. Fractions with a Rz value greater than 1.50 were pooled and concentrated. For the preparation of adamantanone-bound cytochrome P450cam, camphor was removed by passage of the camphor-bound proteins over a Sephadex G-25 column equilibrated with 50 mM MOPS, pH = 7.4 buffer. Then, the substrate-free enzyme solution was saturated with solid adamantanone in the presence of 100 mM KCl. Excess adamantanone was removed by centrifugation. The enzyme preparation was stored under liquid nitrogen until ready for use. Protein concentrations were estimated from the known absorptivity of 102 mM^{-1} cm^{-1} at 391 nm for camphor-bound cytochrome P450cam.

The oxygenated adduct of ferrous cytochrome P450cam was prepared as follows. Approximately 0.2 mL of 100 μM enzyme solution (in either camphor-bound or adamantanone-bound form) was placed in a 5-mm o.d. NMR tube and sealed with a rubber septum. The tube was then flushed with pure nitrogen for 15 min to remove oxygen. A 5-μL volume of buffered aqueous sodium dithionite (about a 10-fold molar excess of reducing agent relative to heme) was added through a syringe. After reduction was complete, oxygen (^{16}O or $^{18}O_2$) was introduced to form the reddish oxygenated derivative. The NMR tube was then immediately frozen by dipping into a dry ice–acetone slurry.

Resonance Raman spectra were acquired with a Spex 1403 spectrometer equipped with Hamamatsu R-928 photomultiplier and a Spex DM1B system controller. Excitation lines at 413.1 nm (from a Coherent Innova Model 100-k3 Kr^+ ion laser) and 441.6 nm (from a Liconix Model 4240NB helium:cadmium laser) were used. For the measurement of oxygenated cytochrome P450cam, the NMR tube containing the frozen sample was quickly transferred to a low-temperature double-walled glass cell of in-house design, and spectra were recorded in a backscattering geometry. Throughout the spectral acquisition, the NMR tube was kept spinning and the temperature was maintained at −80 °C by flushing with prechilled dry nitrogen. The sample of Fe($TP_{piv}P$)($C_6HF_4S^-$)(O_2) and Fe($TP_{piv}P$)($C_6F_5S^-$)(O_2) was prepared according to a modification of a published procedure[17] using the "minibulb" technique.[18]

Results and Discussion

A. Heme Core Vibrational Modes. Figure 1 displays the high-frequency (1300–1700 cm^{-1}) resonance Raman spectra of oxygenated cytochrome P450cam, stabilized at −80 °C, in the presence of camphor (trace A) and adamantanone (trace B). For comparison, a RR spectrum of oxymyoglobin (trace C), recorded under identical conditions, is included. The spectrum shown in trace A agrees well with that reported by Champion et al.[14] and is characteristic of a six-coordinated, low-spin adduct. The most intense feature, the oxidation marker band known as ν_4, is located at 1374 cm^{-1}, a frequency which is slightly lower (3 cm^{-1}) than that of the oxygenated adducts of hemeproteins containing histidyl as a proximal ligand.[19] For example, the ν_4 for oxymyoglobin is observed at 1377 cm^{-1} as shown in trace C. In order to investigate the interaction of substrate with the bound dioxygen, camphor is replaced with adamantanone, an analogue of greater steric bulk. The binding of this substrate analogue to the resting state of cytochrome P450cam shifts its spin state from low to high spin to a degree that is comparable to the effect of camphor binding. The electronic absorption spectrum of oxycytochrome P450cam shows little difference between the adamantanone- and camphor-bound forms and their stability is also comparable. As is shown in trace B of Figure 1, the RR spectrum is essentially the same as trace A, implying an identical heme core structure.

It is well known that excitation into the Soret (or Q) band of the prosthetic group of hemeproteins gives rise to a very rich spectral pattern in the region between 1300 cm^{-1} and 1700 cm^{-1}. These features have been properly assigned to the in-plane vibrational modes of the porphyrin skeleton and those related to the vinyl groups, based on the isotope substitution and normal coordinate analysis.[20] The frequencies are empirically correlated with the heme core size, i.e., the distance of the center-to-pyrrole nitrogen (Ct–N) of the porphyrin cavity, and are very useful in monitoring the spin state and oxidation state of the heme iron.[21] The most prominent feature (ν_4), which can be clearly identified without interference from other modes, is sensitive to the electron population in the π^* antibonding orbitals of the porphyrin ring. The more populated the π^* orbital, the lower the frequency of ν_4. It has been noted previously that an anomalously low frequency of ν_4 is observed for ferrous cytochrome P450 from a variety of sources,[10] presumably owing to the presence of a strong electron-releasing thiolate axial ligand. Analogous, but smaller, shifts are also observed in the high-spin ferric state, ferrous carbon monoxide adduct, and ferric nitrosyl adducts of cytochrome P450cam. It is not surprising that the ν_4, detected at 1374 cm^{-1} for oxygenated cytochrome P450cam, is lower than that of oxymyoglobin. Table I compares the frequencies of the ν_4 mode of cytochrome P450cam and myoglobin in ferric and ferrous states and for the adducts involving π acid ligands (CO, NO, CN^{-1} and O_2). The RR spectra of all the derivatives of myoglobin are recorded under the same conditions as for cytochrome P450cam

Table I. Comparison of ν_4 Frequencies for Various Derivatives of Cytochrome P450cam and Myoglobin

	cytochrome P450cam	myoglobin	reference
Fe(III)	1370	1371	10b
Fe(II)	1345	1357	10a, 10b
Fe(III)–NO	1375	1375	this work, 45
Fe(II)–CO	1368	1373	12a
Fe(II)–NO	1372	1375	this work, 45
Fe(II)–O_2	1374	1377	this work

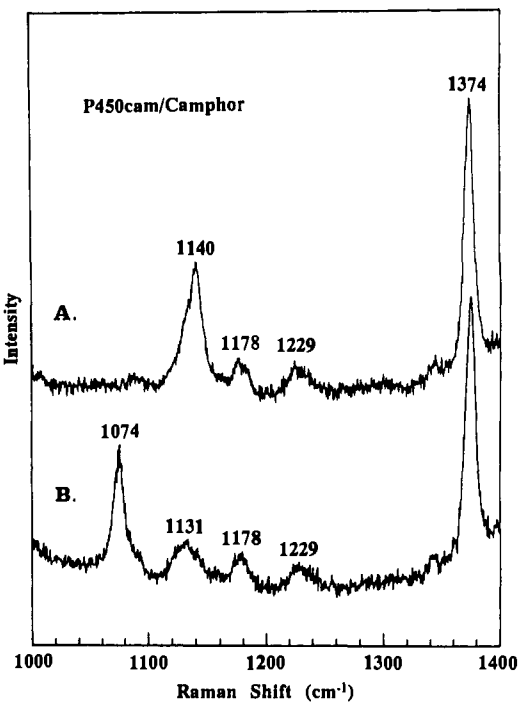

Figure 2. Resonance Raman spectra of dioxygen adduct of camphor-bound cytochrome P450cam in the ν(O–O) region: trace A, $^{16}O_2$; trace B, $^{18}O_2$.

(17) Schappacher, M.; Ricard, L.; Fisher, J.; Weiss, R.; Bill, E.; Montiel-Montoya, R.; Winkler, H.; Trautwein, A. X. *Eur. J. Biochem.* **1987**, *168*, 419–429.

(18) Nakamoto, K.; Nonaka, Y.; Ishiguro, T.; Urban, M. W.; Suzuki, M.; Kozuka, M.; Nishida, Y.; Kida, S. *J. Am. Chem. Soc.* **1982**, *104*, 3386.

(19) (a) Spiro, T. G.; Strekas, T. C. *J. Am. Chem. Soc.* **1974**, *96*, 338. (b) Spiro, T. G.; Burke, J. M. *J. Am. Chem. Soc.* **1976**, *98*, 5482–5489. (c) Kitagawa, T.; Iizuka, T.; Saito, M.; Kyogoku, Y. *Chem. Lett.* **1975**, *8*, 49. (d) Van Wart, H. E.; Zimmer, J. *J. Biol. Chem.* **1985**, *260*, 8372–8377.

(20) (a) Kitagawa, T.; Abe, M.; Ogoshi, H. *J. Chem. Phys.* **1978**, *69*, 4516. (b) Abe, M.; Kitagawa, T.; Kyogoku, Y. *J. Chem. Phys.* **1978**, *69*, 4526. (c) Li, X.-Y.; Czernuszewicz, R. S.; Kincaid, J. R.; Su, Y. O.; Spiro, T. G. *J. Phys. Chem.* **1990**, *94*, 31–46. (d) Li, X.-Y.; Czernuszewicz, R. S.; Kincaid, J. R.; Stein, P.; Spiro, T. G. *J. Phys. Chem.* **1990**, *94*, 47–61.

(21) (a) Spaulding, L. D.; Cheng, C. C.; Yu, N.-T.; Felton, R. H. *J. Am. Chem. Soc.* **1975**, *97*, 2517. (b) Spiro, T. G.; Strong, J. D.; Stein, P. *J. Am. Chem. Soc.* **1979**, *101*, 2648. (c) Choi, S.; Lee, J. J.; Wei, Y. H.; Spiro, T. G. *J. Am. Chem. Soc.* **1983**, *105*, 3692–3707. (d) Parthasarathi, N.; Hanson, C.; Yamaguchi, S.; Spiro, T. G. *J. Am. Chem. Soc.* **1987**, *109*, 3865.

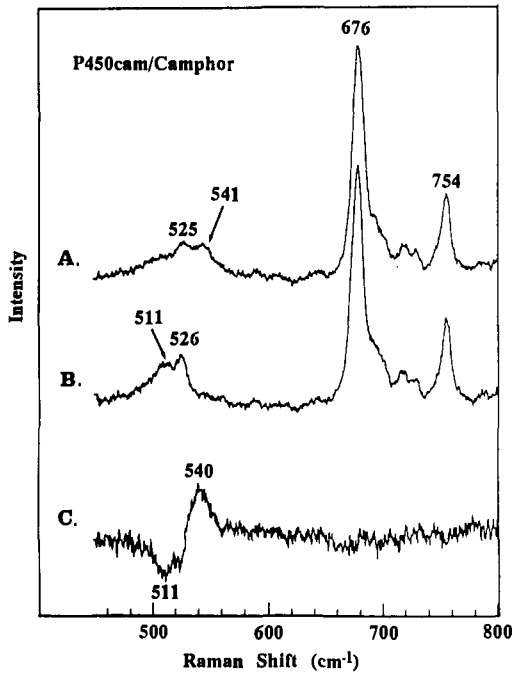

Figure 3. Low-frequency resonance Raman spectra of dioxygen adduct of camphor-bound cytochrome P450cam: trace A, $^{16}O_2$; trace B, $^{18}O_2$; trace C, difference spectrum (A − B) × 2 (traces A and B are normalized relative to the band at 676 cm^{-1}).

in order to eliminate the possible differences reported from different studies.[22] It is clear that a lowered frequency of ν_4 for cytochrome P450cam is preserved for all the derivatives. The smaller difference observed for π-acid liganded forms is a result of the redistribution of the electron density between the π^* orbital of the heme and the axial ligand π^* orbital, which suppresses the dramatic lowering of ν_4 as observed in the case of the ferrous state. These results suggest that the mercaptide axial ligand donates more electron density to the porphyrin ring via the central metal so as to weaken the bond strength of Fe–L bond.

B. Simultaneous Observation of ν(Fe–O_2) and ν(O–O) Modes. Figure 2 shows the RR spectra in the ν(O–O) region of the $^{16}O_2$ and $^{18}O_2$ adducts of ferrous cytochrome P450cam in the presence of camphor. The asymmetrical band at 1140 cm^{-1} (trace A) shifts to 1074 cm^{-1} and becomes a sharp symmetrical peak (trace B) upon $^{16}O_2/^{18}O_2$ substitution. The residual feature at 1136 cm^{-1} is ascribable to an overlapping porphyrin mode as was observed in the case of oxymyoglobin.[23] The observed isotopic shift, essentially the same as the calculated one for an isolated harmonic oscillator model, confirms its assignment as the ν(O–O) mode.[14]

In order to further characterize the oxygenated cytochrome P450cam, we have attempted to locate the important ν(Fe–O_2) mode. Figure 3 illustrates the low-frequency RR spectra of the oxygenated adducts of cytochrome P450cam in the region where the ν(Fe–O_2) mode is likely to occur. The relatively strong bands at 676 cm^{-1} and 754 cm^{-1} can be assigned to the ν_7 and ν_{15} modes of heme skeletal vibrations.[20] In addition, it is noted that when $^{18}O_2$ is used to prepare the oxygenated adduct, the peak at 541 cm^{-1} disappears and a feature centered at 511 cm^{-1} gains intensity (trace B). The difference spectrum (trace C), obtained by normalizing trace A and trace B relative to the ν_7 mode, clearly shows the isotopic sensitivity. Obviously, this new oxygen isotope-sensitive band can be reasonably assigned to ν(Fe–O_2). Thus, both ν(O–O) and ν(Fe–O_2) modes for oxycytochrome P450cam are simultaneously observed.

Previously, simultaneous enhancement of internal O–O stretching and M–O_2 stretching vibrations has been observed only for the Soret excited RR spectra of the oxy adducts of Co(II)-reconstituted hemeproteins[24] and their models.[25] However, the complicated spectral pattern in the ν(O–O) region, which results from the coupling of ν(O–O) and the internal mode of the axially coordinated imidazole,[26] renders it difficult to analyze the factors that may influence the frequencies of ν(Co–O_2) and ν(O–O). For the oxyhemeproteins and their models possessing histidyl or other nitrogen donor axial ligands, no ν(O–O) vibrations have been observed directly by Raman, though an intensity increase at 1125 cm^{-1} upon $^{16}O_2/^{18}O_2$ substitution was noted in the RR spectra of oxy sperm whale myoglobin and oxy elephant myoglobin.[23] A recent RR study of Fe(TPP)O_2, presumably a five-coordinate, high-spin species in oxygen matrices, revealed two isotope-sensitive lines at 1195 cm^{-1} and 509 cm^{-1}, which were assigned to ν(O–O) and ν(Fe–O_2), respectively (based on their isotopic shift).[27] However, this observation is, to some extent, inconsequential for the case of heme proteins, inasmuch as oxyhemeproteins are invariably six-coordinate. The effect of coordination number changes on the enhancement of axial vibrations was also noted for the ferrous nitric oxide adducts of hemeproteins.[28]

The RR enhancement of the ν(O–O) mode in an iron(II) porphyrin–O_2 adduct was first made by Chottard et al.[15] in the RR spectra (with excitation line at 441 nm) of Fe(T_{piv}PP)($C_6HF_4S^-$)(O_2), a model for the oxygenated adduct of cytochrome P450. The frequency of this mode at 1140 cm^{-1} is the same as measured by IR difference spectroscopy.[29] Similarly, the ν(O–O) of the bound dioxygen in oxycytochrome P450cam was also strongly brought out in the RR spectra excited at 420 nm.[14] In both cases, the low-frequency spectra did not show any specific band that is sensitive to oxygen isotope substitution. In contrast, our spectra obtained with excitation line at 413 nm demonstrate clearly the enhancement of both vibrational modes of interest. We note that the intensity of ν(O–O) mode is weaker, relative to ν_4, than that excited at 420 nm. It should be pointed out that the ν(O–O) can also be observed for oxycytochrome P450cam with excitation line 441 nm, and its intensity is comparable to ν_4.

The simultaneous enhancement of both ν(O–O) and ν(Fe–O_2) modes in oxygenated cytochrome P450cam upon the excitation near the Soret absorption is similar to those observations on the cobalt-substituted heme proteins.[24,25] Yu and co-workers[24] suggested that the charge-transfer transition from the occupied π^* to empty antibonding σ^* orbital is responsible for the Raman enhancement of both ν(O–O) and ν(Co–O_2) modes in the dioxygen adducts of cobalt porphyrins. For oxy iron(II) porphyrin adducts, this transition is obviously absent, since the π^* orbital is no longer populated by an electron. The enhancement of the ν(Fe–O_2) mode was proposed to arise from the porphyrin π–π^* transition mechanism, based on the fact that the Raman excitation profile follows the absorption spectrum in both the Soret and Q-band region.[30] However, in oxygenated P450cam and analogues, the strong electron-donating axial ligand, mercaptide, may overlap with this empty π^* orbital (through P_x and d_π) to transfer electrons to the central metal so as to make the iron(II) resemble cobalt(II), thus accounting for the simultaneous enhancement. This argument is further supported by the observation that the frequencies of both ν(O–O) and ν(M–O_2) modes are strikingly close in both systems.

(22) Rimai, L.; Salmeen, I.; Petering, D. H. *Biochemistry* **1975**, *14*, 378–382.
(23) Kerr, E. A.; Yu, N.-T.; Bartnicki, D. E.; Mizukami, H. *J. Biol. Chem.* **1985**, *260*, 8360–8365.
(24) Tsubaki, M.; Yu, N.-T. *Proc. Natl. Acad. Sci. U.S.A.* **1981**, *78*, 3581–3585.
(25) (a) Bajdor, K.; Kincaid, J. R.; Nakamoto, K. *J. Am. Chem. Soc.* **1984**, *106*, 7741–7747. (b) Kincaid, J. R.; Proniewicz, L. M.; Bajdor, K.; Bruha, A. *J. Am. Chem. Soc.* **1985**, *107*, 6775.
(26) (a) Bruha, A.; Kincaid, J. R. *J. Am. Chem. Soc.* **1988**, *110*, 6006–6014. (b) Proniewicz, L. M.; Kincaid, J. R. *J. Am. Chem. Soc.* **1990**, *112*, 675–681.
(27) Wagner, W.-D.; Paeng, I. R.; Nakamoto, K. *J. Am. Chem. Soc.* **1988**, *110*, 5565.
(28) Mackin, H. C.; Benko, B.; Yu, N.-T.; Gersonde, K. *FEBS Lett.* **1983**, *158*, 199–202.
(29) Schappacher, M.; Ricard, L.; Weiss, R.; Montiel-Montoya, R.; Bill, E.; Gonser, U.; Trautwein, A. *J. Am. Chem. Soc.* **1981**, *103*, 7646.
(30) Walters, M. A.; Spiro, T. G. *Biochemistry* **1982**, *21*, 6991–6995.

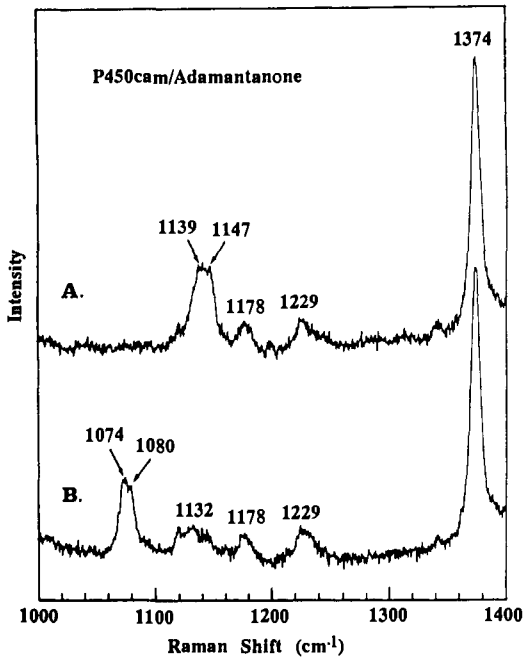

Figure 4. Resonance Raman spectra of dioxygen adduct of adamantanone-bound cytochrome P450cam at −80 °C in the ν(O–O) region: trace A, $^{16}O_2$; trace B, $^{18}O_2$.

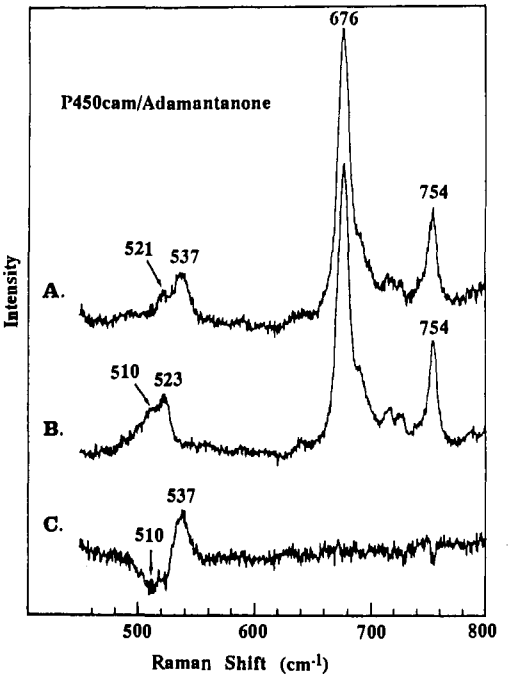

Figure 5. Low-frequency resonance Raman spectra of dioxygen adduct of adamantanone-bound cytochrome P450cam at −80 °C: trace A, $^{16}O_2$; trace B, $^{18}O_2$; trace C, difference spectrum A − B (traces A and B are normalized relative to the band at 676 cm^{-1}).

The frequency (541 cm^{-1}) of the ν(Fe–O_2) mode for oxygenated cytochrome P450cam is remarkably lower than those reported for oxyhemeproteins (567 cm^{-1}),[31] oxymyoglobin (570 cm^{-1}),[23] compound III of horseradish peroxidase (562 cm^{-1}),[19b] and the dioxygen adducts (~570 cm^{-1}) of fully reduced[32] and mixed-valence cytochrome *c* oxidase.[33] The result indicates that the Fe–O_2 linkage in cytochrome P450cam system is substantially weakened. The lowering of iron–ligand vibrational frequency was also noted previously for the ferrous carbonyl[12] and ferric nitrosyl adducts,[13] owing to the presence of strong electron-donating axial ligand.

We note that the isotopic shift (30 cm^{-1}) of the ν(Fe–O_2) mode for oxygenated cytochrome P450cam and several model analogues is somewhat larger than that expected (24 cm^{-1}) for a simple harmonic diatomic vibrator. In addition, a neighboring band at 525 cm^{-1} gains intensity in the spectrum for $^{18}O_2$ adduct (trace B), which can also be seen in the difference spectrum (trace C) as a residual peak. The nonideal isotopic shifts and the appearance of satellite bands in the spectrum are indicative of vibrational coupling of modes associated with the metal–O_2 fragment with modes of the porphyrin or trans-axial ligands.[26b] This behavior is observed in the present work both for the O_2 adducts of protein and for the model compounds (Figures 3, 5, 6, and 8). In addition, O_2 adducts of cobalt-substituted dimeric insect hemoglobin II exhibited similar behavior.[34] While further work would be necessary to identify the source of this coupling in each system, its presence does not invalidate the results and conclusion reported here.

C. Substrate Sensitivity of ν(Fe–O_2) and ν(O–O) Modes. Comparison of Figures 2 and 4 illustrates the effect of substrate replacement (camphor and adamantanone) on the ν(O–O) mode. As discussed earlier, the electronic absorption spectrum and heme core vibrations are identical for the dioxygen adduct in the presence of both substrates. However, the spectral pattern in the ν(O–O) region exhibits a dramatic change. While a single strong feature is observed at 1140 cm^{-1} in trace A of Figure 2, in Figure 8 two peaks of nearly equal intensity (located at 1139 cm^{-1} and 1147 cm^{-1}, respectively) are observed. The identification and assignment of these two bands to the bound dioxygen is confirmed by the shifts observed upon $^{16}O_2/^{18}O_2$ substitution (trace B). Thus, the magnitudes of the observed isotopic shifts (67 cm^{-1} and 65 cm^{-1}) are almost the same as that expected (65 cm^{-1}). In addition, the consequence of substrate change in the ν(Fe–O_2) is also visible in the low-frequency RR spectra of oxygenated adamantanone-bound cytochrome P450cam (Figure 5). The heme modes ν_7 and ν_{15} remain the same, but the spectral feature assigned to the ν(Fe–O_2) mode does exhibit some noticeable differences. First, in trace A the relative intensity of the two peaks at 521 cm^{-1} and 537 cm^{-1} is reversed as compared to trace A of Figure 3. The difference spectrum (trace A) reveals that the oxygen isotope sensitive band is located at 537 cm^{-1}, which is 4 cm^{-1} lower than that of the camphor-bound adduct. It should be pointed out that two ν(Fe–O_2) modes are expected, based on the observation of the two ν(O–O) frequencies. However, the separation of these two bands may be too small to be resolved with these experimental conditions. In any case, the results presented here demonstrate that the vibrational frequencies associated with the bound dioxygen are sensitive to the steric bulk of the substrate and provide direct evidence for its contact with the bound dioxygen.

In the past, the effect of substrate steric bulk on the vibrational characteristics of bound diatomic ligands was recognized only for linear adducts, especially the Fe^{II}–CO fragment. The distortion of Fe–C–O linkage often gives rise to the enhancement of δ(Fe–C–O) mode as is observed in the RR spectra of the CO adducts of heme proteins.[35] The elegant RR studies carried out by Yu and co-workers[36] for the carbon monoxide adducts of strapped porphyrins demonstrate clearly that both the ν(Fe–CO) and ν(C–O) modes are sensitive to the steric hindrance imposed

(31) Brunner, H. *Naturwissenschaften* **1974**, *61*, 129.
(32) (a) Varotsis, C.; Woodruff, W. H.; Babcock, G. T. *J. Am. Chem. Soc.* **1989**, *111*, 6439–6440. (b) Han, S.; Ching, Y.-C.; Rousseau, D. L. *Proc. Natl. Acad. Sci. U.S.A.* **1990**, *87*, 2491–2495. (c) Ogura, T.; Takahashi, S.; Shinzawa-Itoh, K.; Yoshikawa, S.; Kitagawa, T. *J. Am. Chem. Soc.* **1990**, *112*, 5630–5631.
(33) (a) Han, S.; Ching, Y.-C.; Rousseau, D. L. *Biochemistry* **1990**, *29*, 1380–1384. (b) Varotsis, C.; Woodruff, W. H.; Babcock, G. T. *J. Biol. Chem.* **1990**, *265*, 11131–11136.
(34) (a) Yu, N.-T.; Thompson, H. M.; Zepke, D.; Gersonde, K. *Eur. J. Biochem.* **1986**, *157*, 579–583. (b) Mackin, H. C.; Tsubaki, M.; Yu, N.-T. *Biophys. J.* **1983**, *41*, 349–357.
(35) (a) Kerr, E. A.; Yu, N.-T. In *Biological Applications of Raman Spectroscopy*; Spiro, T. G., Ed.; John Wiley: New York, 1988; pp 39–95. (b) Yu, N.-T. *Methods Enzymol.* **1986**, *130*, 350–409.
(36) Yu, N.-T.; Kerr, E. A.; Ward, B.; Chang, C. K. *Biochemistry* **1983**, *22*, 4534–4540.

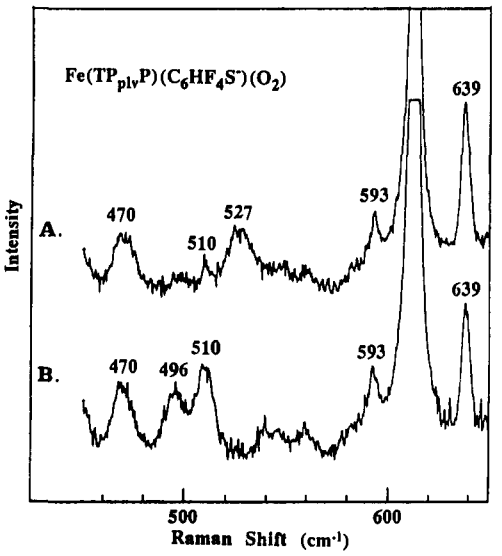

Figure 6. Low-frequency resonance Raman spectra (441.6-nm excitation) of Fe(T$_{piv}$PP)(C$_6$HF$_4$S$^-$)(O$_2$) dissolved in chlorobenzene at −40 °C: trace A, $^{16}O_2$; trace B, $^{18}O_2$.

by the strap above the bound CO molecule. However, a similar work on the dioxygen adduct of the heme[37] failed to detect such frequency shifts of ν(Fe–O$_2$) as the length of handle was varied. However, a lowered frequency at 560 cm^{-1} was observed, which was attributed to the change of Fe–O–O angle.

It has been noted that the binding of substrate controls the spin state and redox potential of ferric heme iron,[38] lowers the ligand affinity of ferrous enzyme for carbon monoxide,[39] and stabilizes the quasi-stable oxygenated cytochrome P450cam.[40] A perturbation of the vibrational frequencies of ν(Fe–XO), δ(Fe–X–O), and ν(X–O) by substrate was previously noted in the RR spectra of the ferrous carbon monoxide[12] and ferric nitric oxide adducts.[13] However, the effect of adamantanone on ν(Fe–CO) and ν(Fe–NO) seems inconsistent. The ν(Fe–CO) mode for adamantanone-bound cytochrome P450cam is observed at 474 cm^{-1}, a frequency that is between those for camphor-bound (481 cm^{-1}) and substrate-free (464 cm^{-1}) forms and is virtually indistinguishable from that of the norcamphor-bound enzyme (a camphor analogue, but of smaller size). On the other hand, a recent RR study of ferric NO adducts suggests that adamantanone binds to the active site more tightly than does camphor, a conclusion which is consistent with the recent X-ray crystal structural determination of adamantanone- and norcamphor-bound cytochrome P450cam.[5d]

The multiple lines observed for the ν(O–O) mode of adamantanone-bound oxygenated cytochrome P450cam can be attributed to the conformational disorder of the Fe–O$_2$ linkage caused by different orientations of adamantanone within the heme pocket. The naturally evolved substrate for this enzyme system, camphor, is held within the active site through its interactions with the protein; in particular, the hydrogen-bonding interaction between the camphor carbonyl oxygen atom and the hydroxyl group of Tyr96 and the "lock-and-key" contact of the geminal dimethyl groups of camphor with Val295 and Leu244.[5c] For the adamantanone-bound adduct, though the hydrogen-bonding interaction is preserved, the lack of complementary methyl groups may allow

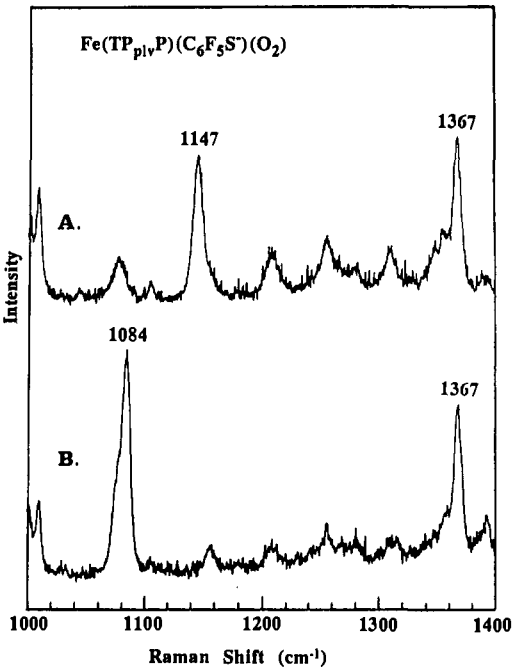

Figure 7. Resonance Raman spectra (441.6-nm excitation) of Fe(T$_{piv}$PP)(C$_6$F$_5$S$^-$)(O$_2$) dissolved in CH$_2$Cl$_2$ at 150 K in the ν(O–O) region: trace A, $^{16}O_2$; trace B, $^{18}O_2$.

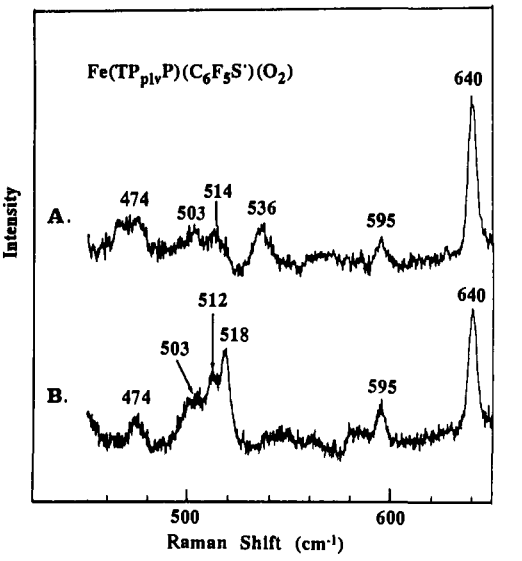

Figure 8. Low-frequency resonance Raman spectra (441.6-nm excitation) of Fe(T$_{piv}$PP)(C$_6$F$_5$S$^-$)(O$_2$) dissolved in CH$_2$Cl$_2$ at −120 °C: trace A, $^{16}O_2$; trace B, $^{18}O_2$.

it to move freely, for example, to rotate about its carbonyl bond. Evidence for such disorder is provided by the recent X-ray crystal structural determination of adamantanone-bound ferric cytochrome P450cam.[5d] It is worthwhile noting that the effect of such a rotation on the distribution of hydroxylated products cannot be determined, owing to the intrinsic symmetry of adamantanone. This rotation may result in two distinct interactions of substrate with the bound dioxygen (i.e., the terminal oxygen atom being directed to and away from the adamantanone molecule), thus giving rise to two ν(O–O) modes.

D. Influence of the Axial Thiolate Ligands on ν(Fe–O$_2$) and ν(O–O) Modes. In an attempt to delineate the various factors that determine the enhancement and frequencies of the ν(Fe–O$_2$) and ν(O–O) modes, we have undertaken a RR study of model compounds. Figure 6 displays the low-frequency RR spectra of the well-known model of the dioxygen adduct of cytochrome P450, Fe(T$_{piv}$PP)(C$_6$HF$_4$S$^-$)(O$_2$). The high-frequency spectra are essentially the same as reported previously,[15] exhibiting a strong

(37) Desbois, A.; Momentean, M.; Lutz, M. *Inorg. Chem.* **1989**, *28*, 825–834.

(38) (a) Sligar, S. G. *Biochemistry* **1976**, *15*, 5399–5406. (b) Fisher, M. T.; Sligar, S. G. *J. Am. Chem. Soc.* **1985**, *107*, 5108. (c) Sligar, S. G.; Gunsalus, I. C. *Proc. Natl. Acad. Sci. U.S.A.* **1976**, *73*, 1078–1082.

(39) Peterson, J. A.; Griffin, B. W. *Arch. Biochem. Biophys.* **1972**, *151*, 427–433.

(40) (a) Ishimura, Y.; Ullrich, V.; Peterson, J. A. *Biochem. Biophys. Res. Commun.* **1971**, *42*, 147–153. (b) Lipscomb, J. D.; Sligar, S. G.; Namtvedt, M. J.; Gunsalus, I. C. *J. Biol. Chem.* **1976**, *251*, 1116–1124. (c) Debey, P.; Balny, C.; Douzou, P. *FEBS Lett.* **1976**, *69*, 231–235, 236–239. (d) Eisenstein, L.; Debey, P.; Douzou, P. *Biochem. Biophys. Res. Commun.* **1977**, *77*, 1377–1383.

Table II. Summary of ν(O–O) and ν(Fe–O_2) Frequencies (cm^{-1}) for the Dioxygen Adducts of Iron Porphyrins

compounds	ν(Fe–O_2)	ν(Fe–O_2)	reference
1. (Phthalocyanato)Fe–O_2	488	1207	46
2. (TPP)Fe–O_2	509	1195	27
3. (TMP)Fe–O_2	522	1171	42
4. (N-MI)($TP_{piv}P$)Fe–O_2	568	1159	47
5. (pip)(TPP)Fe–O_2	575	1157	48
6. (HbA)Fe–O_2	567	1155, 1106	31, 49
7. (Mb)Fe–O_2	572	1148, 1103	50, 49
8. (P450cam)Fe–O_2/camphor	541	1140	this work, 14
9. (P450cam)Fe–O_2/ adamantanone	537	1147	this work
10. ($C_6HF_4S^-$)($TP_{piv}P$)Fe–O_2	527	1140	this work, 15
11. ($C_6F_5S^-$)($TP_{piv}P$)Fe–O_2	536	1147	this work

line at 1140 cm^{-1} which is assigned to the ν(O–O) of the bound dioxygen (the spectrum is not shown here). In the low-frequency region (Figure 6), it is immediately apparent that the band at 527 cm^{-1} is sensitive to oxygen isotope substitution, and therefore is assigned to the ν(Fe–O_2). The isotopic shift (31 cm^{-1}) is comparable to that found for native protein, but still larger than expected.

Figure 7 presents the RR spectra of an analogous model compound, Fe($T_{piv}PP$)($C_6F_5S^-$)(O_2). In this case, a strong peak appears at 1147 cm^{-1}, which shifts to 1084 upon $^{16}O_2/^{18}O_2$ substitution. Obviously, these bands can be assigned to the ν(O–O) of $^{16}O_2$ and $^{18}O_2$ isotopomers, respectively. The low-frequency spectra of the $^{16}O_2$ and $^{18}O_2$ adducts are displayed in Figure 8. The band at 536 cm^{-1} (trace A) disappears in trace B, with a concomitant intensity increase in the 520-cm^{-1} region. Although the complicated features in the ν(Fe–O_2) region prevent the exact determination of its frequency for $^{18}O_2$ adduct, its frequency for the natural abundance oxy adduct can be clearly identified at 536 cm^{-1}. As explained above, all the $^{18}O_2$ oxygenated adducts (either native enzyme or its models) share the same spectral pattern, i.e., a band assignable to ν(Fe–O_2) and a neighboring band with increased intensity upon $^{18}O_2$ substitution.

Table II summarizes the vibrational data for oxy compounds of iron(II) porphyrins whose ν(O–O) and ν(Fe–O_2) frequencies have been detected by either Raman or IR spectroscopy. From consideration of the backbonding scheme associated with the iron–dioxygen bond,[41] it is generally recognized that increasing the strength of the Fe–O_2 bond results in the weakening of O–O, i.e., the higher the ν(Fe–O_2) the lower the ν(O–O), as reflected in Table II. This is illustrated in the plot of ν(O–O) versus ν(Fe–O_2), shown in Figure 9. The regression line is drawn from all the points, except those of cytochrome P450cam and its model compounds, and can be expressed by

$$\nu(\text{O–O}) = -0.60 \times \nu(\text{Fe}^{\text{II}}\text{–O}_2) + 1495\ (\text{cm}^{-1})$$

It is worthwhile pointing out that this regression equation is different from those proposed recently by Kitagawa and coworkers,[42] who grouped only the experimental data acquired in solution. Instead, we have included all the available data (both the solution and solid matrix). This treatment yields an extrapolated ν(O–O) frequency of 1495 cm^{-1} in the limit, ν(Fe–O_2) = 0 cm^{-1}. This frequency is slightly lower than the ν(O–O) of gaseous dioxygen (1551 cm^{-1}), as expected.[42]

The linear plot suggests that the perturbations on the vibrations of the Fe–O_2 linkage in the different environments (for example, in low-temperature matrix or in the proteins) can be traced to the variation of π-bonding interaction between the iron and dioxygen as long as the donor properties of the axial ligand do not change significantly. However, the points corresponding to oxygenated cytochrome P450cam and its analogues (number 7–10) fall below the linear plot, reflecting the strong donor effect of the axial thiolate group. Such a divergence was also noted in the

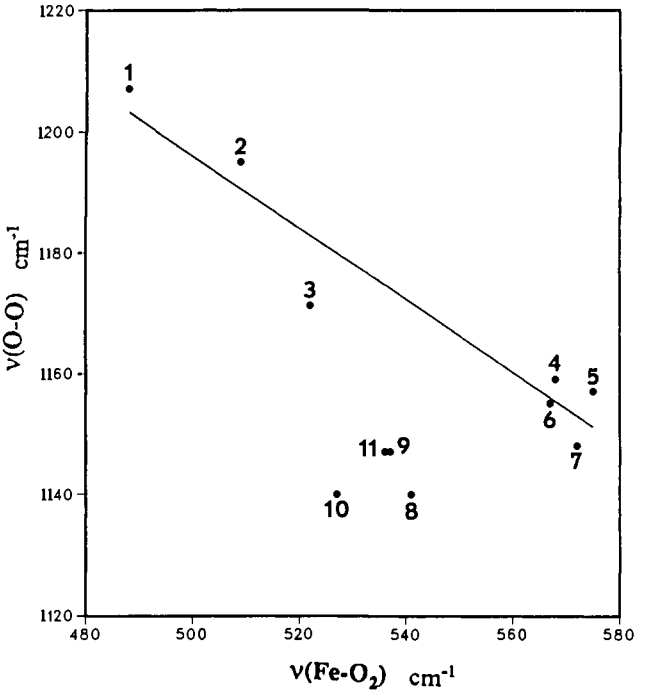

Figure 9. Plot of ν(O–O) versus ν(Fe–O_2) showing the inverse correlation of the two vibrational modes.

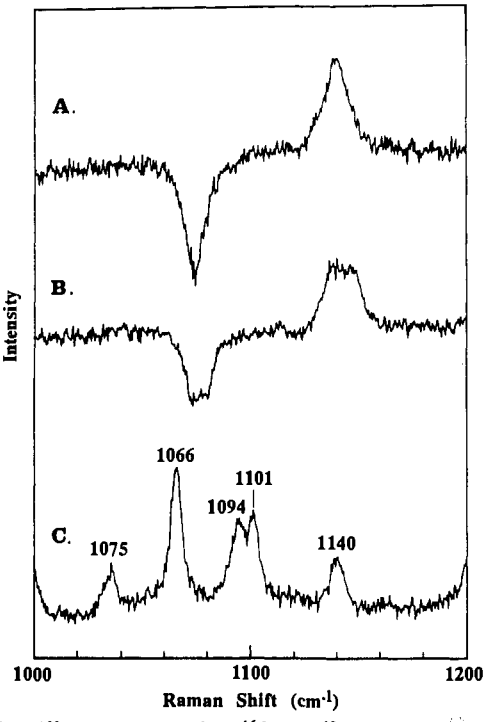

Figure 10. Difference spectra of the $^{16}O_2$ and $^{18}O_2$ adducts of cytochrome P450cam in the presence of camphor (trace A) and adamantanone (trace), obtained by normalizing the respective resonance Raman spectra (shown in Figures 2 and 4, respectively) relative to the 1374-cm^{-1} band. Trace C: Raman spectrum (413.1-nm excitation) of adamantanone dissolved in CH_2Cl_2. The solvent band at 1157 cm^{-1} is subtracted.

vibrational analysis of the carbon monoxide adducts of heme-proteins and iron porphyrins.[43]

E. Evidence for the Enhancement of an Internal Mode of the Bound Adamantanone. Figure 10 shows the difference spectra of the $^{16}O_2$ and $^{18}O_2$ adducts of cytochrome P450cam in the presence of camphor (trace A) and adamantanone (trace B), which are obtained by normalizing the respective traces (shown in Figures

(41) Oertling, W. A.; Kean, R. T.; Wever, R.; Babcock, G. T. *Inorg. Chem.* **1990**, *29*, 2633–2645.

(42) Mizutani, Y.; Hashimoto, S.; Tatsuno, Y.; Kitagawa, T. *J. Am. Chem. Soc.* **1990**, *112*, 6809–6814.

(43) Li, X. Y.; Spiro, T. G. *J. Am. Chem. Soc.* **1988**, *110*, 6024–6033.

2 and 4) relative to the ν_4 (1374 cm^{-1}) mode. These spectra give a clear-cut comparison of the band intensity and width, since the interfering porphyrin modes are canceled out. It is noted that both the $\nu(^{16}O-^{16}O)$ and $\nu(^{18}O-^{18}O)$ regions are broader for the adamantanone-bound adduct relative to camphor. This is due to the presence of two conformers as discussed in the previous section. However, we emphasize here that the bandwidth of the unresolved features in the ν(O–O) region of the $^{16}O_2$ adduct of the adamantanone-bound enzyme (trace B) is significantly broader than that of the $^{18}O_2$ adduct, though the integrated areas of the positive and negative peaks are identical within experimental error. The observation of selective band broadening of one isotopomer ($^{16}O_2$) can be reasonably ascribed to the enhancement of an internal mode of the bound adamantanone. As can be seen in the Raman spectrum of adamantanone (trace C), several bands occur in this region; in particular, the mode at 1140 cm^{-1} is closely energy-matched with the ν(O–O) frequency. The natural substrate, camphor, however, does not exhibit any band in this region (spectrum not shown), and no evidence of a perturbed spectral pattern is indicated in trace A.

Previously, we had demonstrated such an enhancement of the solvent and solute internal mode via the resonance vibrational coupling in the RR spectra of dioxygen adducts of cobalt porphyrins.[44] In that case, we were able to use isotopically labeled solvents (toluene and chlorobenzene) and various nitrogenous bases to fine-tune the frequencies of ν(O–O) and internal modes so as to systematically study their interactions. It was shown that the enhancement requires a close association of the molecule in question with the bound dioxygen and is critically dependent upon energy matching of the mode with the ν(O–O) stretching frequency. Clearly, these two requirements are satisfied for the dioxygen adduct of adamantanone-bound cytochrome P450cam system, and may be responsible for the observed band broadening in the case of $^{16}O_2$ adduct, although further studies using deuterated adamantanone would be needed to unambiguously confirm such coupling.

Acknowledgment. This work was supported by a grant from the National Institutes of Health (DK35153). The authors are sincerely grateful to Professor S. Sligar of the University of Illinois at Urbana—Champaign for the supply of *P. putida* cell paste.

(44) Kincaid, J. R.; Proniewicz, L. M.; Bajdor, K.; Bruha, A.; Nakamoto, K. *J. Am. Chem. Soc.* **1985**, *107*, 6775-6781.
(45) Benko, B.; Yu, N.-T. *Proc. Natl. Acad. Sci. U.S.A.* **1983**, *80*, 7042-7046.
(46) Bajdor, K.; Oshio, H.; Nakamoto, K. *J. Am. Chem. Soc.* **1984**, *106*, 7273-7274.
(47) (a) Burke, J. M.; Kincaid, J. R.; Peters, S.; Gagne, R. R.; Collman, J. P.; Spiro, T. G. *J. Am. Chem. Soc.* **1978**, *100*, 6083-6087. (b) Walters, M. A.; Spiro, T. G.; Suslick, K. S.; Collman, J. P. *J. Am. Chem. Soc.* **1980**, *102*, 6857-6858. (c) Collman, J. P.; Brauman, J. I.; Halbert, T. R.; Suslick, K. S. *Proc. Natl. Acad. Sci. U.S.A.* **1976**, *73*, 3333-3337.
(48) Nakamoto, K.; Paeng, I. R.; Kuroi, T.; Isobe, T.; Oshio, H. *J. Mol. Struct.* **1988**, *189*, 293-300.
(49) (a) Alben, J. O.; Bare, G. H.; Moh, P. P. In *Biochemical and Clinical Aspects of Hemoglobin Abnormalities*; Caughey, W. S., Caughey, H., Eds.; Academic Press: New York, 1978; pp 607-617. (b) Barlow, C. H.; Maxwell, J. C.; Wallace, W. J.; Caughey, W. S. *Biochem. Biophys. Res. Commun.* **1973**, *55*, 91-95. (c) Maxwell, J. C.; Volpe, J. A.; Barlow, C. H.; Caughey, W. S. *Biochem. Biophys. Res. Commun.* **1974**, *58*, 166-171. (d) Brown, W. E., III; Sutcliffe, J. W.; Pulsinelli, P. D. *Biochemistry* **1983**, *22*, 2914-2923.
(50) Tsubaki, M.; Nagai, K.; Kitagawa, T. *Biochemistry* **1980**, *19*, 379-385.

Structural Models for Covalent Non-Oxidic Glasses. Atomic Distribution and Local Order in Glassy $CdGeP_2$ Studied by ^{31}P and ^{113}Cd MAS and Spin-Echo and $^{31}P-^{113}Cd$ Spin-Echo Double Resonance NMR Spectroscopy

Deanna Franke, Robert Maxwell, David Lathrop, and Hellmut Eckert*

Contribution from the Department of Chemistry, University of California, Santa Barbara, California 93106. *Received October 3, 1990*

Abstract: The structure of glassy $CdGeP_2$ is discussed on the basis of complementary solid-state NMR experiments, including ^{31}P and ^{113}Cd magic-angle spinning (MAS) and spin-echo techniques, as well as $^{31}P-^{113}Cd$ spin-echo double resonance (SEDOR) NMR. Modeling of the dipolar interactions in conjunction with experimental studies on the crystalline model compounds CdP_2 and $CdGeP_2$ reveals the short-range order present in crystalline $CdGeP_2$ is not preserved upon vitrification. In contrast to the crystalline analogue, glassy $CdGeP_2$ contains a substantial fraction of phosphorus–phosphorus bonds, which can be quantitated by means of ^{31}P spin-echo decay data. The analysis reveals that the number of P–P bonds amounts to 55 ± 5% of that expected for a completely random distribution of atoms. The $^{113}Cd-^{31}P$ SEDOR results are qualitatively consistent with this conclusion but suggest a more complete randomization of the Cd atoms. As a consequence of this randomization of atomic occupancies, the number of Cd–P bonds is significantly reduced in the glassy state. The study provides important experimental data for the development of realistic atomic distribution models for covalent non-oxidic glasses.

Introduction

The development of novel materials with properties suitable for applications as low-frequency infrared waveguides still represents a major challenge in materials science. Most of the work carried out so far has concentrated on non-oxidic glasses, based on fluoride, sulfide, and selenide anions.[1] For many of these systems, however, the good optical properties are compromised by major drawbacks such as low glass transition temperatures and a pronounced air and moisture sensitivity. It has been much less widely realized that there exists a whole class of potentially superior materials, based on phosphides and arsenides of main-group and post-transition elements. These glasses are sometimes called the "chalcopyrite glasses", since their prototype compounds exhibiting glass formation, $CdGeAs_2$ and $CdGeP_2$, both crystallize in the chalcopyrite structure. Most importantly from the ap-

(1) Taylor, P. C. *Mater. Res. Soc. Bull.* **1987**, 36. Andriesh, A. M. *J. Non-Cryst. Solids* **1985**, *77/78*, 1219.

0002-7863/91/1513-4822$02.50/0